

## **Supporting Information for**

### **Graphene Annealing: How Clean Can It Be?**

Yung-Chang Lin,<sup>1</sup> Chun-Chieh Lu,<sup>1</sup> Chao-Huei Yeh,<sup>1</sup> Chuanhong Jin,<sup>2</sup> Kazu Suenaga,<sup>2</sup> Po-Wen Chiu<sup>1\*</sup>

<sup>1</sup>Department of Electrical Engineering, National Tsing Hua University, Hsinchu 30013, Taiwan

<sup>2</sup>National Institute of Advanced Industrial Science and Technology (AIST), Tsukuba 305-8565, Japan

#### **TEM specimen preparations and measurements**

TEM images presented in this work were carried out on CVD graphene grown on a same Cu foil to avoid quality variations. To transfer graphene, a thin layer of PMMA prepared using chloroform as solvent was spun on the Cu foil, followed by wet etching in a FeCl<sub>3</sub> aqueous solution. The PMMA, along with the attached graphene sheet, was then transferred onto a Mo grid (Quantifoil). For the samples that combine TEM with Raman measurements, gold patterns were made on graphene by e-beam lithography, followed by the same transfer process to TEM holey grids. The PMMA was first removed by acetone, followed by annealing. Electron microscopy characterizations were conducted using a JEOL 2100F transmission electron microscope equipped with a cold field emission gun and two DELTA correctors. Acceleration voltage of 60 kV was used throughout the measurements with specimens at ambient temperature. The TEM images were recorded by a Gatan CCD (model 894) with a typical exposure time of 1 second.

#### **Raman Measurements**

Micro-Raman spectra were obtained on both Si-supported and free-standing CVD

graphene using a commercial Raman microscope (HR800, HORIBA). Measurements were performed at room temperature with a laser excitation wavelength of 633 nm. A 100x objective was used to provide a diffraction-limited spot size of approximately 1  $\mu\text{m}$ . A low power level ( $< 1 \text{ mW}$ ) was used to avoid any heating effect. Lorentzian fits were used throughout the Raman spectra presented in Fig. 6.

### **Graphene annealing**

Figure S1 shows the TEM images of graphene annealed at 300  $^{\circ}\text{C}$  in air for 1 h, followed by another hour of annealing in the flow of mixed  $\text{H}_2$  (200 sccm) and Ar (400 sccm). Except the temperature, other annealing conditions are the same with that presented in Fig. 2–4. The image scales in Fig. S1 are the same with those in Fig. 2–3. Compared with the graphene annealed at 250  $^{\circ}\text{C}$  (Fig. 3), the most obvious difference is the decrease of metal residues on graphene after raising the temperature. No apparent macroscopic damages such as tears and cracks are induced by the migration of metal particles at this temperature. For graphene annealed at 300  $^{\circ}\text{C}$ , both PMMA-A and PMMA-G have similar densities with those annealed at 250  $^{\circ}\text{C}$ , i.e., no apparent difference in cleanliness between graphene annealed at 250  $^{\circ}\text{C}$  and 300  $^{\circ}\text{C}$ . However, it does not imply that the intrinsic graphene properties are similar. Figure S2 and S3 show the TEM images of graphene annealed in a flow of mixed  $\text{H}_2$  (200 sccm) and Ar (400 sccm) for 200  $^{\circ}\text{C}$  and 300  $^{\circ}\text{C}$ , respectively. For the annealing at 200  $^{\circ}\text{C}$ , the graphene surface is still covered by PMMA-G, and it is difficult to find clean areas. Raising the temperature to 250  $^{\circ}\text{C}$  under the same annealing conditions do help in cleanliness. This is due to the fact that PMMA-G starts burning at higher temperatures.

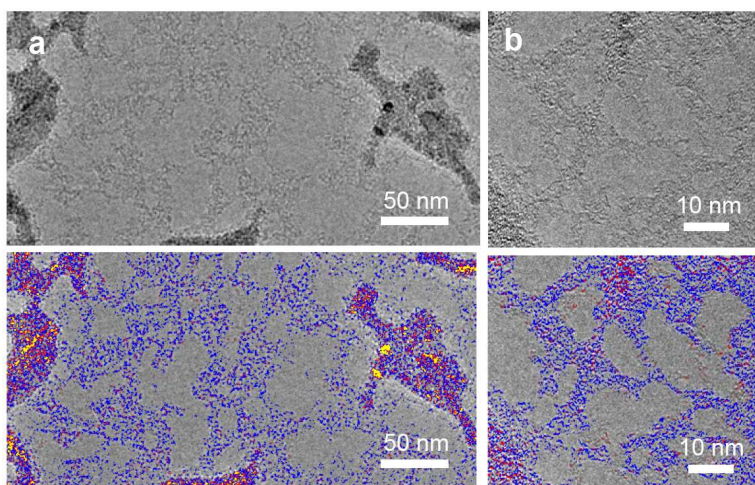


Figure S1. TEM images of graphene after air/H<sub>2</sub> two-step annealing at 300 °C for 1 h for each step. (a) and (b) show the details of surface cleanliness. The same images are duplicated and colored in the lower panels to distinguish the different layers of PMMA residues that decomposed differently. The coloring is the same as that in the schematics of Fig. 2. The areas free of PMMA are shown in grey in the colored images.

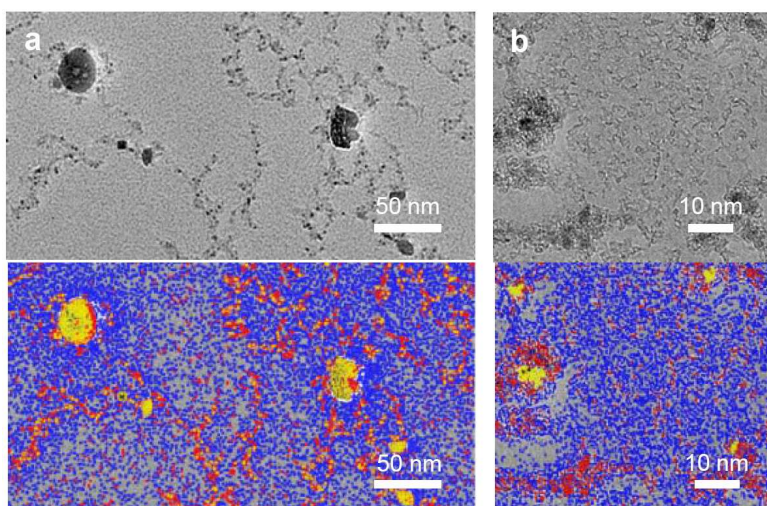


Figure S2. TEM images of graphene after H<sub>2</sub>/Ar one-step annealing at 200 °C for 2 h. (a) and (b) show the details of surface cleanliness. The same images are duplicated and colored in the lower panels. The coloring is the same as that in the schematics of Fig. 2. The areas free of PMMA are shown in grey in the colored images.

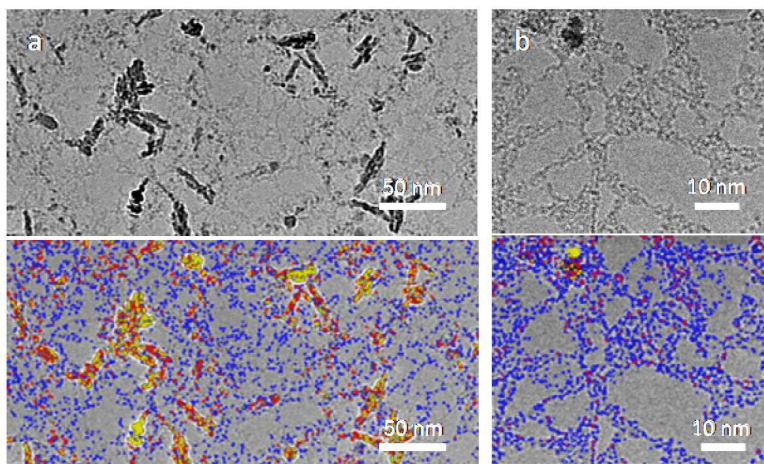


Figure S3. TEM images of graphene after H<sub>2</sub>/Ar one-step annealing at 250 °C for 2 h. (a) and (b) show the details of surface cleanliness. The same images are duplicated and colored in the lower panels. The coloring is the same as that in the schematics of Fig. 2. The areas free of PMMA are shown in grey in the colored images.

### DFT calculations

To gain insight into the electronic structure of the MMA-graphene complex, the pseudo-potential density functional SIESTA package was used for calculations,<sup>1-4</sup> with the local density approximation (LDA) representing the exchange correlation potential and with an energy mesh cutoff of 200 Ry. The generalized gradient approximation was only used as the reference of the binding energy's lower bound because it tends to yield much lower binding energies. The Brillouin zone was sampled with a grid of 6×6×1 k-points within the Monkhorst-Pack scheme.<sup>5</sup> The band structure of the MMA-graphene complex was calculated using 10×10 supercell containing 200 carbon atoms with MMA placed on top. A 15 Å vacuum inter-layer separation of molecules in different cells ensured negligible interaction between one graphene layer and its periodic images. The molecule/graphene system was fully optimized by allowing all the system's degrees of freedom to relax until the force acting on each atom was below 0.04 eV/ Å and total energies were below 1 meV. During optimization, the electronic ground state was found self-consistently. Fig.

S4 shows three different optimized adsorption configurations with corresponding band structures displayed in Fig. S5.

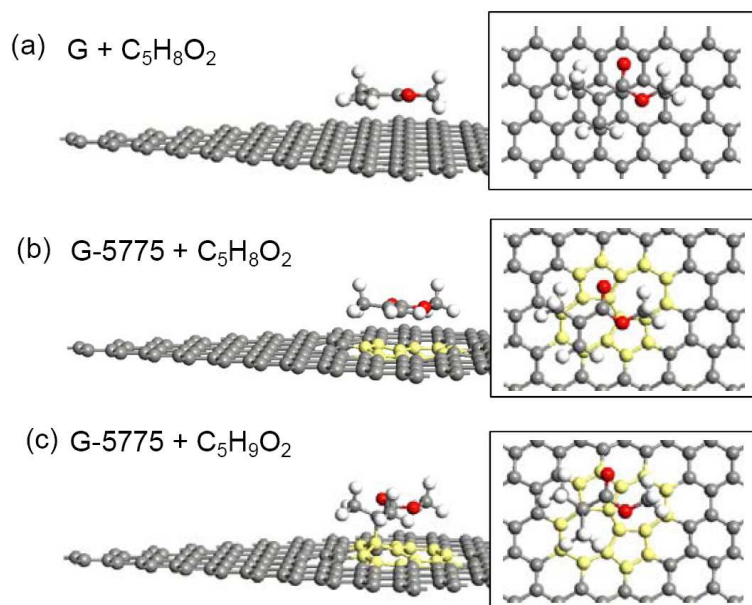


Fig. S4(a) Side and top view of the optimized adsorption of MMA ( $C_5H_8O_2$ ) on ideal graphene. (b) A Stone-Wales defect (5775 pair) is introduced in the graphene supercell. (c) The macroradical, represented by  $C_5H_9O_2$ , form a covalent bond with graphene on top of the Stone-Wales defect.

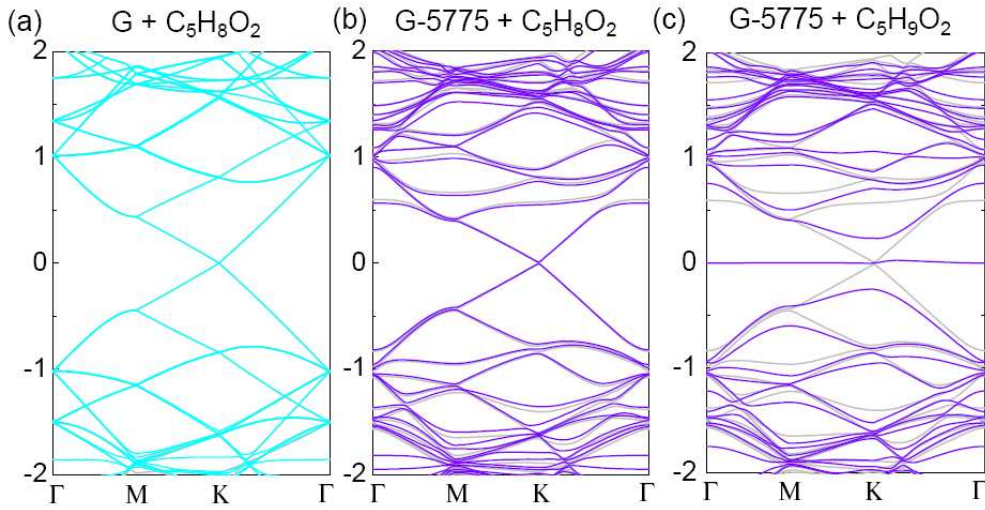


Fig. S5 Band structures of different MMA-graphene complexes shown in Fig. S4. The band structures of pristine graphene are shown in grey for comparison. (a) The band structure of MMA ( $\text{C}_5\text{H}_8\text{O}_2$ ) adsorption on ideal graphene coincides very well with that of pristine graphene at low energy, indicative of a negligible interaction between MMA and graphene. (b) Introduction of a Stone-Wales defect in the graphene supercell does not cause significant changes in the band structure as compared with the case in (a). (c) An energy gap appears due to the local rehybridization of carbons from  $sp^2$  to  $sp^3$  and hence a remarkable reduction of the Fermi velocity near the **K** points.

## References

- [1] Quantum Wise A/S, "Atomistix Tool Kit", **2010**, Ch. 10.8.2.
- [2] M. Brandbyge, J. Mozos, P. Ordejón, J. Taylor, K. Stokbro, *Phys. Rev. B* **2002**, *65*, 165401.
- [3] J. M. Soler, A. Emilio, J. D. Gale, A. Garcia, J. Junquera, P. Ordejon, D. Sanchez-Portal, *J. Phys. : Condens. Matter* **2002**, *14*, 2745.
- [4] J. Taylor, H. Guo, J. Wang, *Phys. Rev. B* **2001**, *63*, 245407.
- [5] H. J. Monkhorst, J. D. Pack, *Phys. Rev. B* **1976**, *13*, 5188.